Convection-Diffusion with the Colour Gradient Lattice Boltzmann Method for Three-Component, Two-Phase Flow

Convection-Diffusion with the Colour Gradient Lattice Boltzmann Method for Three-Component, Two-Phase Flow

Noname manuscript No.
(will be inserted by the editor)

Convection-diffusion with the colour gradient Lattice Boltzmann Method for three-component, two-phase flow

Peter Mora · Gabriele Morra · Dave A. Yuen · Shirish Patil · Ruben Juanes

February 2, 2023

P. Mora
Geosciences Department
College of Petroleum Engineering and Geosciences
King Fahd University of Petroleum and Minerals
Dhahran, 31261, Saudi Arabia
Tel.: +966-13-860-2566
Fax: +966-13-860-2595
E-mail: wolop2008@gmail.com

G. Morra
Department of Physics, University of Louisiana at Lafayette
104 E University Ave, Lafayette, LA, 70504, U.S.A.
Tel: +1-337-482-6692
Fax: +1-337-482-6699
E-mail: morra@louisiana.edu

D. Yuen
Dept. of Applied Physics and Applied Mathematics, Columbia University
New York, NY 10027, U.S.A.
Tel: +1-651-206-8659
Fax: +1-212-854-8257
E-mail: daveyuen@gmail.com

and

Dept. of Information Science and Engineering and College of Marine Geosciences
Ocean University of China, 238 Songling Road, Qingdao, 266100, China
Tel: +86-188-2762-2561
E-mail: daveyuen@gmail.com

· S. Patil
Petroleum Engineering Department
College of Petroleum Engineering and Geosciences
King Fahd University of Petroleum and Minerals
Dhahran, 31261, Saudi Arabia
Tel.: +966-13-860-2566
Fax: +966-13-860-2595
E-mail: patil@kfupm.edu.sa

Abstract The Rothman-Keller (RK) colour gradient Lattice Boltzmann Method (LBM) provides a means to simulate two phase flow of immiscible fluids by modelling number densities of two fluids, plus a "recoloring" step that ensures separation of the two fluids. Here, we model an additional number density representing the concentration of an additive to fluid 1 which affects the viscosity of this fluid. The Peclet number – rate of advection to diffusion – is used to set the diffusion coefficient of the concentration. We present tests to demonstrate the method including flow and merging of two adjacent droplets with different additive concentrations, and two-phase flow tests in a 2D porous matrix involving injection of fluid with an additive that increases the viscosity and thus decreases viscous fingering (eg. a polymer additive). We demonstrate that use of polymers from the start of waterflooding leads to a high saturation of 90% much sooner than when polymers are applied after breakthrough. This work demonstrates that the RK color gradient multiphase LBM can be used to study viscous fingering behavior in porous media in which the injected low viscosity fluid can have its viscosity varied with time by use of an additive. This is both of scientific interest and has economic implications to Enhanced Oil Recovery (EOR), in which water – potentially with a polymer additive to increase viscosity – is injected from an injection well into a rock layer saturated with a high viscosity fluid (oil) to help push out the oil into a production well.

1 Introduction

Viscous fingering, the formation of narrow tendrils of an invading fluid, occurs when water – which has a low viscosity – is injected into a porous medium saturated by crude oil which has a much higher viscosity (Homsy, 1997[13]; Måløy et al., 1985[22]; Chen and Wilkinson, 1985[4]; Lenormand et al., 1988[21]). These patterns of viscous fingering pose a major challenge for Enhanced Oil Recovery (EOR) by waterflooding, as the narrow fingers reduce the final saturation at breakthrough when these fingers reach the production well. As such, the saturation and hence Recovery Factor (RF) is relatively low and the majority of the oil remains within the porous matrix at the time of breakthrough. For this reason, petroleum engineers have developed various methods to improve the yield of oil reservoirs by EOR post breakthrough. Namely, surfactants may be used to increase the wettability of water after breakthrough which broadens the viscous fingers and as such, increases the sweep (Deng et al., 2020[7]). Use of surfactants in this way is based on numerous laboratory experiments which indicate that sweep increases when the invading fluid's wettability is increased (Kennedy et al., 1955[17]; Jadhunandan and Morrow, 1995[16]; Seethepalli

R. Juanes
Dept. of Civil and Environmental Engineering
Massachusetts Institute of Technology
Cambridge, MA, 02139, U.S.A
Tel: +1-617-253-7191
E-mail: juanes@mit.edu

et al., 2004[29]; Trojer et al., 2015[32]; Zhao et al., 2016[37]). Alternatively, or subsequently, polymers additives can be used which increase the viscosity ratio which decreases the viscous fingering effect and hence, increases the sweep and RF (Abdini et al., 2012[1]). Numerous approaches to directly model multiphase flow at the pore scale have been proposed and applied as summarized by Blunt et al., 2013[3] including the Lattice Boltzmann Method (LBM), Smoothed Particle Hydrodynamics, the level set method and traditional approaches to solve the Navier-Stokes equations. Density functional modelling (Armstrong et al., 2016[2]; Demianov et al., 2011[8]) has also been applied to pore scale modelling of multiphase flow with different properties including polymer flooding (Yakimchuk et al., 2020[34]). It is beyond the scope of this paper to review these methods and their relative strengths which has already been done by Blunt et al., 2013[3]. Here we focus on how to extend the a popular Lattice Boltzmann Method for multiphase flow – the Rothman-Keller color gradient LBM (Rothman and Keller, 1988[28]) – to enable polymers to be modelled.

This paper is a continuation of our past numerical simulation research (Mora et al., 2021b[24],2021c[25]) in which we applied the Rothman-Keller (RK) colour gradient Lattice Boltzmann Method (LBM) for two-phase flow to the study of viscous fingering. As before, we chose the RK LBM over other popular multiphase LBM's such as Shan and Chen multi-component multiphase LBM [30], free-energy based multiphase LBM's [31]), Inamuro's multiphase LBM [15], and the He-Chen-Zhang multiphase LBM [12], due to the RK LBM's ability to handle large viscosity ratios, a wide range – over ten orders of magnitude – of surface tensions (Mora, 2021a[23]), and its accuracy and convenience of setting the wetting angle. Huang et al, 2015[14] and Yang and Boek, 2013[35] both provide a summary and comparison of the main multiphase LBM's and their cababilities. We note that phase field methods Wang et al., 2019[33] can also handle large viscosity contrasts, Yang et al., 2013[35], and have been used for studies of viscous fingering such as Zacharoudiou et al., 2020[39]. Hence, phase field methods could also be adapted in the same way as is done in this paper, to include an extra number density for a polymer concentration which affects the viscosity. However, for the reasons given above, we have chosen the RK LBM but we have no opinion as to which LBM method may be "better". The colour gradient LBM has been validated against various analytic solutions as in Huang et al., 2015[14] and Yang and Boek, 2013[35].

Our previous numerical simulation studies using the colour-gradient Lattice Boltzmann Method (LBM) to simulate two-phase flow (Mora et al., 2021b,2021c[24, 25]) have shown that the saturation at breakthrough is a complex function of wettability, viscosity ratio and porous medium geometry and may contain hills and valleys. Mora et al., 2021c[25] showed the saturation landscape as a function of wettability and viscosity ratio is affected by the structure of the porous medium, and that viscous fingers continue to expand and evolve post breakthrough. Hence, the RF continues to increase beyond breakthough. One of the major results of these past studies was that the dominant effect on suppressing viscous fingering, and thus increasing saturation (RF) is the viscosity ratio.

Here, we utilize the colour-gradient Lattice Boltzmann Method (LBM) to simulate two-phase flow with a new variable representing polymer concentration, which affects the viscosity of the injected fluid in order to enable studies to be conducted of how the sweep evolution is affected by use polymer additives. Hence, we describe a model for convection-diffusion of three-component, two-phase flow using the color-gradient LBM. We then conduct tests to verify the method and present a comparison study of the effect on the saturation evolution using polymers additives before and after breakthrough when injecting a low viscosity fluid (cf. water), into a model porous matrix saturated with a high viscosity fluid (cf. crude oil).

2 Review of the colour-gradient LBM

In this paper, we extend the Rothman-Keller (RK) multiphase Lattice Boltzmann model for immiscible two-phase flow which was originally derived for a Lattice Gas Automaton (Rothman and Keller, 1988;[28]; Gunstensen et al., 1991[11]), and later extended to the Lattice Boltzmann Method (LBM) by Latva and Kokko, 2005[19]. The RK colour gradient Lattice Boltzmann Method involves modelling particle distributions denoted f_α^k of two fluids moving and colliding on a discrete lattice. The total number density of the two phase fluid is given by

$$f_\alpha(\mathbf{x},t) \;=\; \sum_k f_\alpha^k(\mathbf{x},t) \quad ,$$

where the subscript α specifies the direction in the lattice, and the superscript $k = 1, 2$ denotes fluid 1 and fluid 2 often denoted the "red" and "blue" fluids.

There are three steps in this method to model the two number densities of the fluids which are (i) streaming, (ii) collision, and (iii) "recolouring". The streaming step is the same as the standard Lattice Boltzmann Method streaming step. Namely, in one time-step, the particle distributions move by one lattice spacing along the orthogonal axes, or along diagonals. We use the standard LBM notation $DnQm$ for a simulation in $D = n$ dimensions, and with $Q = m$ velocities on the discrete lattice. In the following, we restrict ourselves to 2D and use the $D2Q9$ Lattice Boltzmann lattice arrangement. In this lattice, we define $f_\alpha^k(\mathbf{x},t)$ as the number density of particles of fluid k moving in the α-direction where the $Q = 9$ velocities are given by

$$\begin{aligned}\mathbf{c}_\alpha = [&(0,0),(1,0),(-1,0),(0,1),(0,-1),\\ &(1,1),(-1,-1),(1,-1),(-1,1)]\Delta x/\Delta t\end{aligned}$$

This choice means that $\mathbf{c}_0$ is the zero velocity vector and therefore represents stationary particles, and $\mathbf{c}_\alpha$ for $\alpha = (1,\ldots,8)$ are the velocities in the eight directions lattice directions as defined above which means that $\mathbf{c}_\alpha = -\mathbf{c}_{\alpha+1}$ for $\alpha = (1,3,5,7)$. The lattice is unitary so the lattice spacing and time step are $\Delta x = \Delta t = 1$. The streaming step is specified as

$$f_\alpha^k(\mathbf{x},t) \;=\; f_\alpha^k(\mathbf{x}-\mathbf{c}_\alpha\Delta t, t-\Delta t) \quad , \tag{1}$$

The collision step for the two-phase LBM involves two terms and can be written as (Latva and Kokko, 2005[19])

$$f_\alpha^{k*}(\mathbf{x},t) \;=\; f^k(\mathbf{x},t) \;+\; (\Delta f_\alpha^k)^1 \;+\; (\Delta f_\alpha^k)^2 \quad , \tag{2}$$

where the superscript * denotes the post collision distributions, and $(\Delta f_\alpha^k)^1$ and $(\Delta f_\alpha^k)^2$ are the two collision terms which represent how the particle distributions change during each time step due to collision $(\Delta f_\alpha^k)^1$ while encouraging colour segregation $(\Delta f_\alpha^k)^2$. The first collision term is nearly the same as the standard collision term of the LBM and is given by

$$(\Delta f_\alpha^k)^1 \;=\; \frac{1}{\tau}\left(f_\alpha^{k,eq}(\mathbf{x},t) \;-\; f_\alpha^k(\mathbf{x},t)\right) \tag{3}$$

where τ is the relaxation time and $f_\alpha^{k,eq}(\mathbf{x},t)$ is the equilibrium distribution which is given by

$$\begin{aligned} f_\alpha^{k,eq} &= \rho_k\left(C_\alpha^k + w_\alpha\left[\frac{\mathbf{c}_\alpha\cdot\mathbf{u}}{c_s^2} + \frac{(\mathbf{c}_\alpha\cdot\mathbf{u})^2}{2c_s^4} \;-\; \frac{\mathbf{u}^2}{2c_s^2}\right]\right) \;= \\ &= \rho_k\left(C_\alpha^k + w_\alpha\left[3(\mathbf{c}_\alpha\cdot\mathbf{u}) + \frac{9}{2}(\mathbf{c}_\alpha\cdot\mathbf{u})^2 - \frac{3}{2}\mathbf{u}^2\right]\right) \end{aligned} \tag{4}$$

where $c_s = \Delta x/(\sqrt{3}\Delta t) = 1/\sqrt{3}$ is the speed of sound in the lattice. The above equilibrium distribution is the same as the standard equilibrium distribution except for the rest factor C_α instead of w_α. The coefficients C_α are given by (Grunau et al., 1993[10])

$$C_\alpha \;=\; \begin{cases} \alpha_k & \alpha = 0 \\ \frac{1-\alpha_k}{5} & \alpha = 1,2,3,4 \\ \frac{1-\alpha_k}{20} & \alpha = 5,6,7,8 \end{cases} \quad , \tag{5}$$

where α_k is a parameter that enables the density of the two fluids to be adjusted (Grunau et al., 1993[10]; Reis and Phillips, 2007[27]) and is given by

$$\frac{\rho_{1i}}{\rho_{2i}} \;=\; \frac{1-\alpha_2}{1-\alpha_1} \quad , \tag{6}$$

where ρ_{1i} and ρ_{2i} are the initial densities of fluid 1 and fluid 2. The other weights are the same as the standard LBM. Namely, $w_0 = 4/9$, $w_\alpha = 1/9$ for $\alpha = 1,2,3,4$ and $w_\alpha = 1/36$ for $\alpha = 5,6,7,8$. The macroscopic density of the two fluids are given by

$$\rho_k \;=\; \sum_\alpha f_\alpha^k \quad , \tag{7}$$

the total density of the fluid is given by

$$\rho = \sum_k \rho_k \quad , \tag{8}$$

and the momentum of the fluid is given by

$$\rho \mathbf{u} = \sum_k \sum_\alpha f_\alpha^k \mathbf{c}_\alpha \quad . \tag{9}$$

The relaxation time τ_k relates to the kinematic viscosity ν_k of each fluid as follows

$$\nu_k = c_s^2(\tau_k - 0.5)\Delta t \quad . \tag{10}$$

At the interface between fluids, the relaxation time changes abruptly, which cannot be handled well numerically. Therefore, in order for the relaxation parameter to change smoothly at the interface, it is interpolated as follows Grunau et al., 1993[10]

$$\tau(\mathbf{x}) = \begin{cases} \tau_1 & \psi > \delta \\ g_1(\psi) & 0 < \psi \le \delta \\ g_2(\psi) & -\delta \le \psi \le 0 \\ \tau_2 & \psi < -\delta \end{cases} \quad , \tag{11}$$

where ψ is given by

$$\psi(\mathbf{x}) = \frac{\rho_1(\mathbf{x}) - \rho_2(\mathbf{x})}{\rho_1(\mathbf{x}) + \rho_2(\mathbf{x})} \quad , \tag{12}$$

and $g_1(\psi) = s_1 + s_2\psi + s_3\psi^2$, $g_2(\psi) = t_1 + t_2\psi + t_3\psi^2$, $s_1 = t_1 = 2\tau_1\tau_2/(\tau_1+\tau_2)$, $s_2 = 2(\tau_1 - s_1)/\delta$, $s_3 = -s_2/(2\delta)$, $t_2 = 2(t_1 - \tau_2)/\delta$ and $t_3 = t_2/(2\delta)$. In these equations, the positive free parameter δ affects interface thickness and is usually set as $\delta = 0.98$.

The second collision term is more complex and there are several forms in the literature. Here, we use the term as written in Reis and Phillips[27]

$$(\Delta f_\alpha^k)^2 = A|\mathbf{F}| \left(w_\alpha (\cos(\lambda_\alpha)|\mathbf{c}_\alpha|)^2 - B_\alpha \right) \quad , \tag{13}$$

where $\mathbf{F}(\mathbf{x}, t)$ is the colour gradient, λ_α is the angle between $\mathbf{F}(\mathbf{x}, t)$ and $\mathbf{c}_\alpha$ and A is a parameter that controls the interfacial tension. The colour gradient $\mathbf{F}(\mathbf{x}, t)$ is calculated according to Mora, 2020a[23] which optimizes isotropy of the colour gradient as

$$\mathbf{F}(\mathbf{x}, t) = \sum_\alpha b_\alpha \mathbf{c}_\alpha \left(\rho_1(\mathbf{x} + \mathbf{c}_\alpha \Delta t, t) - \rho_2(\mathbf{x} + \mathbf{c}_\alpha \Delta t, t) \right) \quad , \tag{14}$$

where the $\mathbf{c}_\alpha$ are the velocities and b_α are scalar coefficients of the finite difference approximation of the gradient that is accurate to second order, namely

$$b_\alpha = \begin{cases} \frac{1}{W} & \alpha = 1, 2, 3, 4 \\ \frac{w}{W} & \alpha = 5, 6, 7, 8 \end{cases} \quad , \tag{15}$$

W is given by

$$W = 2 + 4w \quad , \tag{16}$$

and $w = 0.3$ is the weight given to diagonal nearest neighbours relative to orthogonal nearest neighbours in the finite difference calculation of the gradient. Choice of the value of $w = 0.298$ optimizes isotropy of the gradient at small radius of curvature interfaces such as those that occur in flow through a porous medium (Mora et al., 2020a[23]) for the choice of the interfacial thickness parameter $\beta = 0.5$ which will be described shortly. This choice of w has an order of magnitude better isotropy than the standard choice of $w = 1$ from the original paper on the RK colour gradient LBM given by Latva and Kokko[19], and a factor of two superior isotropy for small radius of curvature interfaces such as those occurring in porous flow than the choice of $w = 0.25$ derived by Leclaire et al.[20] based on obtaining isotropic errors in the gradient calculation to second order. As such, the choice of $w = 0.298$ is optimal to obtain the most accurate pore scale phenomenology which require isotropy of the colour gradient and hence surface tension, to correctly capture behaviour such as viscous fingering, droplet formation and other pore scale phenomena.

In Equation (13), the cosine term is given by

$$\cos(\lambda_\alpha) = \frac{\mathbf{c}_\alpha \cdot \mathbf{F}}{|\mathbf{c}| \cdot |\mathbf{F}|} \quad , \tag{17}$$

and $B_0 = -4/27$, $B_\alpha = 2/27$ for $\alpha = 1, 2, 3, 4$ and $B_\alpha = 5/108$ for $\alpha = 5, 6, 7, 8$. Reiss and Phillips[27] have shown that the above parameters yield the correct term for interfacial tension σ in the Navier-Stokes equations.

The final step in the Lattice Boltzmann Method for two phase flow is a so-called "recolouring" step, which achieves separation of the two fluids. This is achieved as follows (Latva and Kokko, 2005[19])

$$f_\alpha^1 = \frac{\rho_1}{\rho} f_\alpha^* + \beta \frac{\rho_1 \rho_2}{\rho^2} f_\alpha^{eq}(\rho, \mathbf{u} = 0) \cos(\lambda_\alpha) \quad , \tag{18}$$

and

$$f_\alpha^2 = \frac{\rho_2}{\rho} f_\alpha^* - \beta \frac{\rho_1 \rho_2}{\rho^2} f_\alpha^{eq}(\rho, \mathbf{u} = 0) \cos(\lambda_\alpha) \quad , \tag{19}$$

where $f_\alpha^* = \sum_k f_\alpha^{k*}$, and A and $\beta \in (0, 1]$ are adjustable parameters that affect the interfacial properties. Namely, β affects the interfacial thickness, and A and τ_1 and τ_2 affect the interfacial tension. That is, parameter A controls the surface tension, but surface tension in the model is also affected by the two viscosities ν_1 and ν_2, and hence τ_1 and τ_2. One must conduct a numerical experiment of a static droplet and apply the Young-Laplace formula for a given set of viscosities ν_1 and ν_2 to obtain the exact relationship between A and surface tension at that set of viscosities. In the above recolouring equation, the equilibrium distribution at zero velocity is given by the standard equilibrium distribution, namely

$$f_\alpha^{eq}(\rho, \mathbf{u} = 0) = w_\alpha \rho \quad .$$

The pressure in the flow field is obtained from the equation of state and can be calculated as

$$p \;=\; c_s^2 \rho \quad .$$

In the Lattice Boltzmann Method, one achieves no-slip boundary conditions by "bounce-back" boundary conditions at the solid interface. Namely, particle number densities bounce back in the direction they came from at fluid-solid interfaces. The RK model for two phase flow allows any wetting contact angle θ_w to be specified by setting the densities of the two fluids in the solid region through (Latva and Kokko, 2005[19])

$$\theta_w \;=\; \cos^{-1}\left(\frac{\rho_{w1} - \rho_{w2}}{\rho_i}\right) \quad , \tag{20}$$

where ρ_{w1} is the density of fluid 1 in the solid regions, ρ_{w2} is the density of fluid 2 in the solid regions, and ρ_i is the initial density of the majority component = ρ_2.

3 The convection-diffusion colour-gradient LBM

In this paper, in order to model a solute within fluid 1 that affects its viscosity (cf. polymer additives), we also model a third number density denoted f_c representing the number density for an additive's concentration (ie. the solute concentration) in fluid 1 (the solvent). Namely, we model movement f^c using the streaming step given by

$$f_\alpha^c(\mathbf{x}, t) \;=\; f_\alpha^c(\mathbf{x} - \mathbf{c}_\alpha \Delta t, t - \Delta t) \quad , \tag{21}$$

and collision step is given by

$$f_\alpha^{c*}(\mathbf{x}, t) \;=\; f_\alpha^c(\mathbf{x}, t) \;+\; \Delta f_\alpha^c \quad , \tag{22}$$

where f_α^{c*} is the number density after collision and Δf_α^c is the collision term given by

$$\Delta f_\alpha^c \;=\; \frac{1}{\tau_c}\left(f_\alpha^{c,eq}(\mathbf{x}, t) \;-\; f_\alpha^c(\mathbf{x}, t)\right) \tag{23}$$

where τ_c is the relaxation time for the solute concentration and the equilibrium distribution $f^{c,eq}$ is the standard equilibrium distribution given by

$$\begin{aligned} f_\alpha^{c,eq} &= \rho_c w_\alpha \left(1 + \frac{\mathbf{c}_\alpha \cdot \mathbf{u}}{c_s^2} + \frac{(\mathbf{c}_\alpha \cdot \mathbf{u})^2}{2c_s^4} \;-\; \frac{\mathbf{u^2}}{2c_s^2}\right) \;= \\ &= \rho_c w_\alpha \left(1 + 3(\mathbf{c}_\alpha \cdot \mathbf{u}) + \frac{9}{2}(\mathbf{c}_\alpha \cdot \mathbf{u})^2 - \frac{3}{2}\mathbf{u}^2\right) \end{aligned} \tag{24}$$

where ρ_c is the macroscopic concentration of the solute which can be computed from the concentration number densities using

$$\rho_c \;=\; \sum_\alpha f_\alpha^c \quad . \tag{25}$$

The above scheme is known to lead to convection diffusion for the concentration ρ_c. Namely, the above LBM equations model the convection diffusion equation in the macroscopic limit (Krüger et al., 2017[18]) given by

$$\frac{\partial C}{\partial t} + \nabla \cdot (C\mathbf{u}) = \nabla \cdot (\kappa \nabla C) \quad , \tag{26}$$

where $C = \rho_c$ is the concentration of the additive, $\mathbf{u}$ is the velocity of the fluid flow, and $\kappa = \nu_c$ is the diffusivity (diffusion coefficient for the solute). That the above equations lead to the convection-diffusion equation has also been verified by comparison of LBM numerical solutions against analytic solutions such as by Zhang et al., 2022[36] which suggest the accuracy of the LBM is typically in the range of $10^{-2} \rightarrow 10^{-3}$ (Tables 1 and 2, plus Figure 3).

3.1 Evaluation of the solvent viscosity and relaxation time

In the fluid collision term given by Equation (3), the relaxation time must be set according to the fluid densities ρ_1 and ρ_2 and viscosities ν_1 and ν_2 using Equation (11). In this work, we assume there is a known equation relating the viscosity ν_1 of fluid 1 to the concentration of the solute denoted $C = \rho_c$ so we have that the viscosity in fluid 1 is a function of concentration so $\nu_1 = \nu_1(\rho_c)$. In the following, the viscosity of fluid 1 as a function of solute concentration is calculated as a simple linear function as

$$\nu_1(C) = \nu_1^0 + (\nu_2 - \nu_1^0)C \quad , \tag{27}$$

where ν_1^0 is the viscosity of fluid 1 with no polymer additive and the polymer concentration is allowed to vary in the range of $C \in [0, 1]$. Hence, when $C = 1$, fluid 1 will have the same viscosity as fluid 2, and when $C = 0$, it will have the viscosity of fluid 1 with no additives. The above simple relationship is used here as our aim is to test the methodology for simulation convection-diffusion in the two-phase LBM. In applied studies, one can adapt the above equation for $\nu_1(C)$ according to lab measurements of this function.

To calculate the relaxation time for the concentration denoted τ_c in Equation (23), we make use of the relationship

$$\nu_c = c_s^2(\tau_c - 0.5)\Delta t \quad , \tag{28}$$

where $\nu_c = \kappa$ is the diffusivity of the additive concentration and can be calculated from a knowledge of the Peclet number which relates to the rate of advection to diffusion and is given by

$$\nu_c = \frac{uL}{Pe} \quad , \tag{29}$$

where Pe is the Peclet number, u is the fluid velocity, and L is the scale length. Hence, using Equation (10), we have for fluid 1 regions

$$\tau_c = \frac{\nu_c}{c_s^2 \Delta t} + 0.5 \quad . \tag{30}$$

In the RK LBM, the density ρ_1 of fluid 1 is approximately ρ_{1i} in the fluid 1 regions, and grades to zero across a boundary to the fluid 2. In our scheme, the concentration is modelled everywhere within all fluid regions according to Equations (21) and (23), and we use the standard LBM bounce-back scheme at solid boundaries. Hence, we do not modify the diffusion equation depending on whether one is within fluid 1 where $\rho_1 \sim \rho_{1i}$ versus fluid 2 where $\rho_1 \sim 0$. However, this would mean that a region of fluid 1 that is disconnected from another region of fluid 1 can have concentrations "leak" between these separate regions (eg. two separate droplets of fluid 1 with different concentrations C). We avoid such leakage through the steps detailed below.

We consider that the boundary between fluid 1 and fluid 2 occurs when $\rho_1 = 0.5\rho_{1i}$, so fluid 1 regions are defined as $\rho_1 \geq 0.5\rho_{1i}$. As such, we wish to create a barrier at this boundary such that diffusion across this boundary does not occur. This is achieved by first calculating – within fluid 2 regions adjacent fluid 1 – the average concentration of nearest neighbours within fluid 1. We then set the number densities f_α^c in this boundary region to be equal to the equilibrium number densities $f_\alpha^{c,eq}$. Namely, we calculate

$$C_{edge}(\mathbf{x}) \;=\; \frac{\sum_\alpha L_1(\mathbf{x}+\Delta\mathbf{x}_\alpha) C(\mathbf{x}+\boldsymbol{\Delta}\mathbf{x}_\alpha)}{\sum_\alpha L_1(\mathbf{x}+\Delta\mathbf{x}_\alpha)} \quad , \tag{31}$$

where $C_{edge} = (\rho_c)_{edge}$ is the calculated concentration within fluid 2 regions that are adjacent to fluid 1 regions (ie. average of adjacent fluid 1 concentrations), L_1 is a logical variable defining fluid 1 regions (ie. L_1 is true if $\rho_1 \geq 0.5\rho_{1i}$, and $\Delta\mathbf{x}_\alpha = \mathbf{c}_\alpha \Delta t$ is the distance between adjacent nodes in the α direction. This barrier is effective in halting solute concentrations within fluid 2 regions from entering fluid 1 regions, and is accurate provided the simulation is relatively close to equilibrium, especially as the region affected is just one lattice node wide, and is anyway updated each time step depending on the adjacent fluid 1 concentration densities f_α^c. In addition to the above method, we set the diffusivity and hence viscosity ν_c to be very small in regions where $\rho_1 \sim 0$. Namely, we set the viscosity ν_c to be small in regions which are essentially absent of the solvent (fluid 1), ie. where $\rho_1 < \delta\rho_{1i}$ where $\delta\rho_1 = 0.001\rho_{1i}$ (ie. nearly 100% fluid 2 regions). This means that in regions which are composed almost entirely fluid 2, we effectively do not allow concentrations to diffuse. Hence, totally disconnected regions fluid 1 will have the solute regions entirely disconnected. We therefore set ν_c in these near 100% fluid 2 regions as

$$\nu_c \;=\; \frac{uL}{Pe_{high}} \quad , \tag{32}$$

where Pe_{high} is a large Peclet number. In the following tests, we set $Pe_{high} = 10^4$. The above approach ensures that disconnected droplets or fingers of fluid 1 with different solute concentrations do not have any effect on one another. It is only when such disconnected regions touch (ie. two droplets are separated by only 1 lattice site so C_{edge} will be the average of the two droplets concentration), that the concentrations between the two droplets will start to diffuse.

4 Merging droplets test calculations

In order to test the method described above for ensuring adjacent droplets do not leak solute concentrations between one another until they touch, we performed a test simulation involving two droplets that eventually merge. This was achieved by initializing a 301×121 lattice with fluid 2 plus with two square regions of fluid 1 that are sufficiently close to one another that they eventually merge as the square regions become circular due to surface tension. The left droplet of fluid 1 is initialized with a solute concentration of $C = 0$, whereas the right droplet of fluid 1 is initialized with a solute concentration of $C = 1$. The boundary conditions are periodic in the y-direction and we use velocity and pressure boundary conditions respectively at the left and right boundaries using Zhou and He's method[38]. Namely, we inject from the left with a velocity of $u_{in} = 0.02$, and set the outlet pressure to be constant at the right boundary. We set viscosities to be $\nu_1 = 0.1$ and $\nu_2 = 0.2$, densities to $\rho_1 = \rho_2 = 1$, the interfacial tension parameter $A = 0.05$ (so strong surface tension) and the Peclet number of the solute is set to be $Pe = 50$.

Figure 1 shows snapshots of the polymer concentration during the simulation showing the details of droplets moving, becoming circular due to surface tension, and merging as the two very close circular droplets feel one another. The dark blue in the plot represents regions of fluid 2 where $\rho_1 < 0.5$. One can see that at $t = 3250$, the two droplets are not quite touching and as such, each droplet remains with its initial solute concentration. At $t = 3300$, the two droplets are "touching" which means that there is only one lattice spacing separating the two droplets where $\rho_1 \geq 0.5\rho_{1i}$. By $t = 3350$, the droplets have started to merge and diffusion occurs of the solute concentration in the newly merged droplet. Subsequent snapshots show the evolution of the solute concentration as the new single merged droplet evolves and becomes circular due to surface tension. This test verifies our method for ensuring that non-touching regions of fluid 1 do not allow leakage of solute between them, and remain as separate entities until they touch and merge.

Figure 2 shows the same time snapshots but visualizing solute concentrations in regions of fluid 1 where $\rho_1 \geq 0.001\rho_{1i}$ and hence, where solute concentrations can diffuse (ie. where $Pe = 50$ in fluid 1 is used to set the diffusivity). Hence, dark blue regions in this figure represent regions of nearly 100% fluid 2 where the diffusivity is set to a very small value calculated from $Pe_{high} = 10^4$. Comparing these images with those in Figure 1, we can see that even when the fluid droplets are separated by a number of lattice sites as shown in the previous figure, there is a small amount of fluid 1 and solute diffusion will occur in these edge regions where $\rho_1/\rho_{1i} \in [0.001, 0.5)$. However, the barrier described above not allow the solute concentrations in these edge regions from affecting the concentrations within these droplet (ie. where $\rho_1 \geq 0.5$) until they touch. We believe the above method is a good approximation for how droplet solute concentrations interact at the edges of droplets in the framework of the LBM where fluid boundaries are not sharp. Also, it must be stated that the following simulations involve injection of fluid 1 continuously with and without an

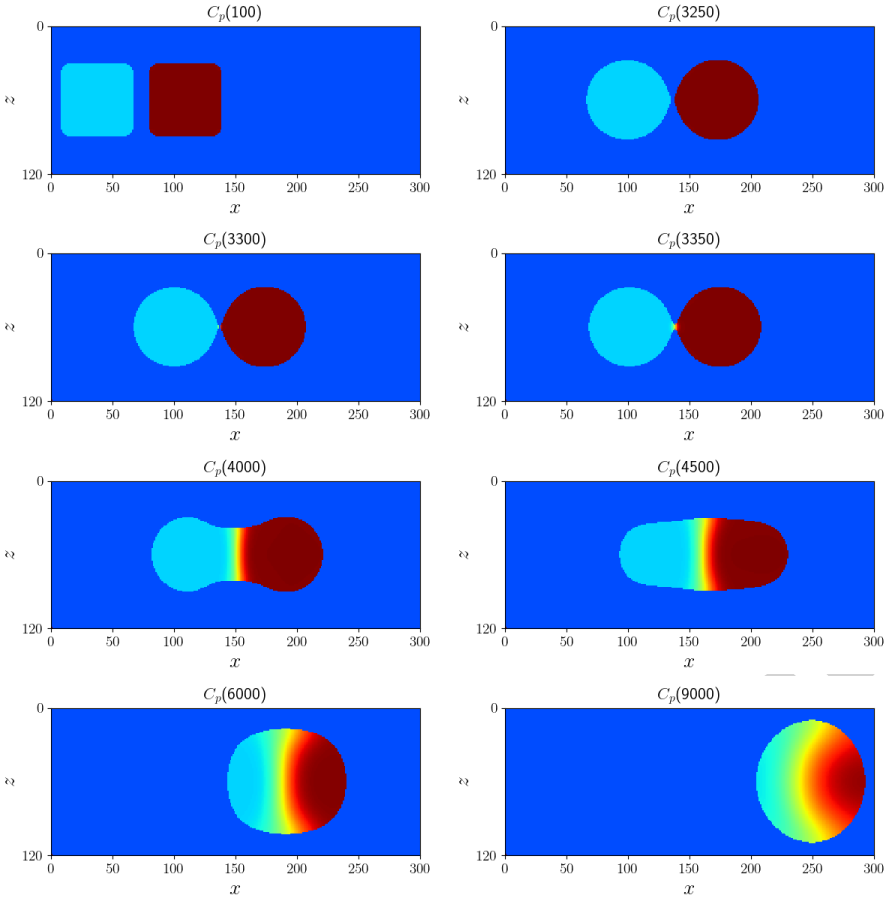

Fig. 1 The evolution of two separate droplets (fluid 1) with different polymer concentration and hence different viscosities, flowing to the right and coalescing. Colors from aqua to red represent fluid 1 regions with concentrations of 0 through 1, and the dark blue color indicates regions of fluid 2. Fluid 1 regions are defined as regions with $\rho_1/\rho_{1i} \geq 0.5$.

additive and hence, there are no significant regions of adjacent droplets with differing solute concentrations. As such, any inaccuracy in the above barrier method will have a negligible effect on the following results.

4.1 Conservation of solute mass

As a final test, we verified that the mass of the solute was conserved during the above droplet merge test. We calculated the total mass of the solute as

$$m = \int_V \rho_1 C \, dV \quad , \tag{33}$$

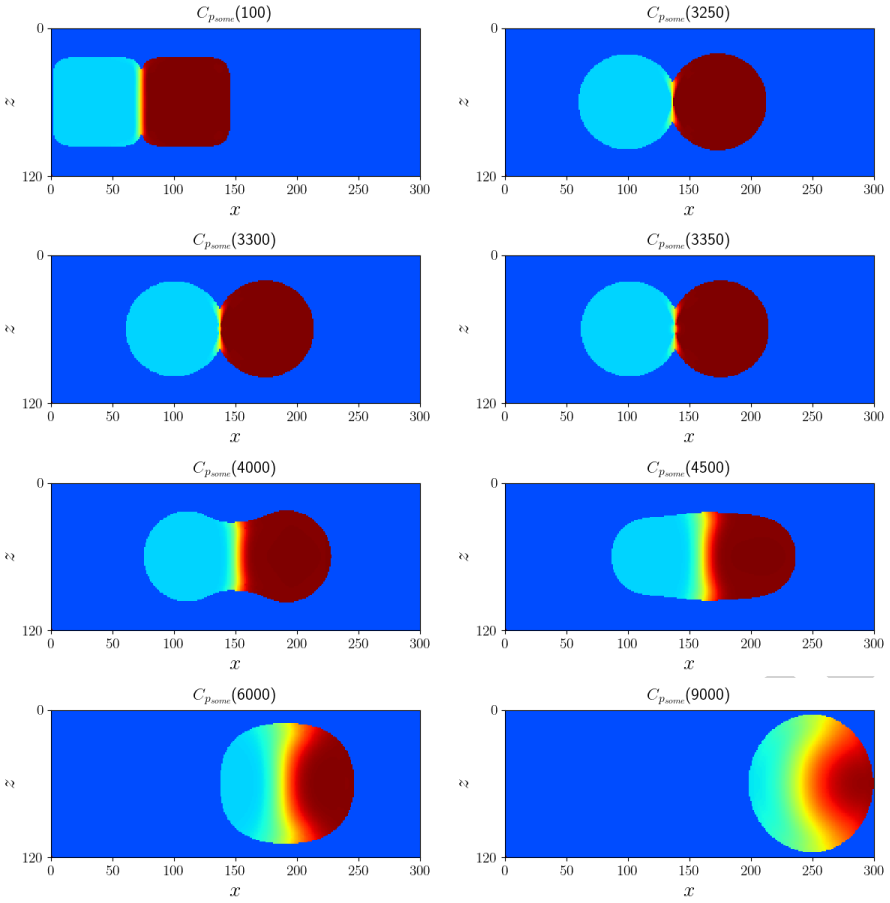

Fig. 2 The evolution of two separate droplets (fluid 1) with different polymer concentration and hence different viscosities, flowing to the right and coalescing. Colors from aqua to red represent fluid 1 and adjacent regions with concentrations of 0 through unity, and the dark blue color indicates regions of fluid 2. Fluid 1 and adjacent regions here are defined here as regions with $\rho_1/\rho_{1i} \geq 0.001$, c.f. the usual definition of fluid 1 regions with $\rho_1/\rho_{1i} \geq 0.5$ as shown in Figure 1.

where ρ_1 is the fraction of fluid 1 at any point containing the solute, and $\boldsymbol{C}$ is the concentration of the solute. The normalized total solute mass defined as

$$m_n = \frac{m}{\bar{m}} \quad , \tag{34}$$

where $\bar{m}_n$ is the mean of m, and we calculated the standard deviation resulting in

$$m_n = 1 \pm 0.0014 \quad , \tag{35}$$

demonstrating that solute mass is conserved to an accuracy of 0.0014. Figure 3 shows a plot of the normalized total solute mass and the error bars indicating

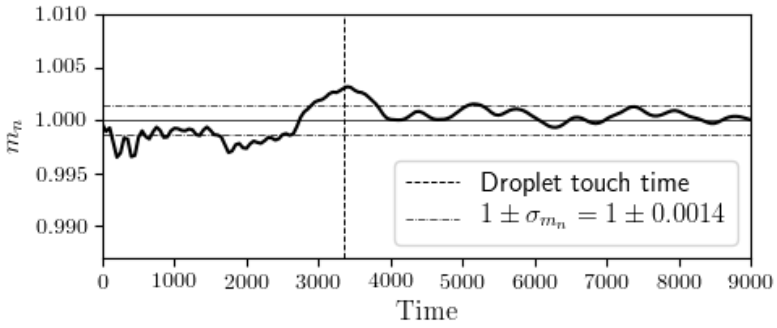

Fig. 3 The normalized solute mass versus time in the droplet merge test.

that there are no sharp changes at the droplet touch time, and that the errors are small.

5 Two phase flow in porous media: effect of polymer usage after breakthrough versus initially

The following sections present tests of the method and examples involving a low viscosity non-wetting fluid (cf. water) with and without polymer additives being injected into a porous rock matrix in 2D that is initially saturated by a high viscosity fluid (cf. crude oil). We choose a non-wetting case as an example here since the viscous fingering is strongest for the non-wetting case. However, in practical studies, one would set the wetting angle of the injected water appropriately for a specific oil field. These tests include a reference comparison of the case of injection both with and without polymer additives always, and a subsequent comparison of the cases of polymer additives being used for a period of time from the start time $t = 0$ versus after the breakthrough time $t = t_{br}$. These studies are conducted at a low viscosity ratio of $M = \nu_1/\nu_2 = 0.01 \sim \nu_{water}/\nu_{crude\ oil}$ at an injection rate that is fast enough to ensure simulations are in the viscous fingering regime, while being low enough to ensure inertia and turbulence are negligible.

5.1 Model setup

As in previous studies (Mora et al., 2021b,2021c[24, 25]), we initialized a square region of 300×300 pixels by dropping random sized circular grains with radii between $5\Delta x$ and $15\Delta x$, such that only those grains separated from other grains by at least $4\Delta x$ are accepted. While this results in a model with unrealistically high porosity compared to real 3D media, it nonetheless ensures the 2D granular medium has significant permeability, and hence, we will be able to model viscous fingering. This model rock matrix was initially saturated by a"blue" fluid with a high viscosity of $\nu_2 = 2$ (representing crude oil). A "red" fluid with

a low viscosity of $\nu_1 = 0.02$ (representing water) is then injected from the left boundary at a constant rate, while the pressure at the right boundary is fixed. Hence, we are modelling the case of a viscosity ratio of $M = \nu_1/\nu_2 = 0.01$ which is a typical viscosity ratio for injected water (the "red" fluid) into a porous model saturated with crude oil (the "blue" fluid). We note that strong viscous fingering occurs when $\nu_1 \ll \nu_2$ and similar results would be obtained using an even lower viscosity ratio (Mora et al., 2021b[24]). The constant injection rate (left BC) and constant pressure (right BC) boundary conditions were achieved using the Zhou and He boundary conditions [38]. Upper and lower boundaries were periodic.

The densities of the fluids were identical with $\rho_1 = \rho_2 = 1$ which is appropriate here considering that the density of water and oil is similar and as such, does not play a significant role in the viscous fingering behaviour. The surface tension parameter A in Equation (13) was set in such a way that the capillary number was high with $Ca \sim 5$, well above the capillary to viscous fingering transition. Namely, the capillary number is given by

$$Ca = \frac{\rho_1 \nu_1 u_{in}}{\sigma} \quad . \tag{36}$$

In the above, ρ_1 and ν_1 are respectively the kinematic viscosity and density of the invading fluid, and u_{in} is the injection rate. And σ denotes surface tension. The value of A in Equation (13) relates to surface tension as

$$\sigma = \alpha A \quad . \tag{37}$$

where parameter α above for a given set of viscosities ν_1 and ν_2 is calculated via numerical simulation of a static droplet through the Young-Laplace formula

$$\sigma = \frac{\Delta P}{r_0} = \frac{P_{in} - P_{out}}{r_0} \quad , \tag{38}$$

where ΔP is pressure differential of a droplet with radius r_0.

We require slow flow rates so that inertia and turbulence are negligible. Hence, we specify a low enough Reynolds number – a dimensionless quantity defined as

$$Re = \frac{u_{in} L}{\nu_1} \quad . \tag{39}$$

where L is the scale length. Hence, we set parameters such that $Re = 0.2 \ll Re_{turbulence} = 2300$. Namely, using a scale length of $L = 4 =$ minimal throat width in the model, we obtain

$$u_{in} = \frac{Re \nu_1}{L} = 0.001 \quad . \tag{40}$$

We note that the choice of the high Capillary number of approximately 5 was merely to ensure we are in the viscous fingering regime. The inlet injection rate u_{in} was chosen to be as high as possible (to minimize compute time), while being low enough to ensure inertial effects are negligible (ie. Reynolds number

$Re = 0.2$). These two conditions – being in the viscous fingering regime and being in the non-inertial regime – ensure we will have the same dynamics of flow as for real oil reservoirs.

5.2 Reference cases: no polymer versus using polymer additives

Figure 4 shows snapshots of the fluid flow in the porous matrix for the case where no polymer additive is used, so at $\nu_1/\nu_2 = 0.01$ where fluid 1 is non-wetting so $\theta_w = 180°$ as a reference case showing the patterns of viscous fingering just after breakthrough at $t = 85K$ (cf. $t_{br} = 84,360$) and beyond. We see strong viscous fingering but notice that post-breakthrough, the fingers continue to evolve and broaden so saturation continues to increase. However, it takes a long time to achieve high saturations (ie. $t \geq 500K \gg t_{br}$).

In contrast, if polymer additives are used from the start that increase the viscosity ratio to unity as shown in Figure 5, we observe what is close minimal fingering so almost stable displacement, and hence much higher saturation at the same time relative to the case of no polymers.

The above cases are equivalent to the specific cases of $M = 0.01$ and $M = 1$ for the non-wetting case shown in the phase space study by Mora et al., 2021b;2021c[24,25], and are shown again here for reference to the simulations in the next section where the effect on saturation evolution of using polymer additives for a duration $\Delta t_{polymer} = t_{br}$ after breakthrough and from $t = 0$ are studied.

5.3 Use of polymer additives after versus before breakthrough

Polymer additives can be used in enhanced oil recovery by waterflooding to increase the viscosity of water, and hence, decrease the viscosity ratio thereby decreasing viscous fingering and improving the recovery factor (RF) – percentage of oil that is recovered (Abdini et al., 2012[1]). This is frequently done after breakthrough is achieved when water first reaches the production well, but can also be done at the start of waterflooding. In the following tests, the convection-diffusion RK LBM described above is used to study and compare these two cases of using polymer additives after breakthrough versus from the start of waterflooding for the same duration $\Delta t_{polymer} = t_{br}$. We compare these two options for using polymer additives after breakthrough or from the start of waterflooding with the reference cases shown in Figures 4 and 5 (ie. (no polymer and always use polymer).

Figure 6 shows snapshots of the polymer concentration for the case of use of polymer additives after the breakthrough time t_{br} for a duration of $\Delta t_{polymer} = t_{br}$. The snapshots show that at $t = 85K \sim t_{br}$, the viscous fingering is identical to the reference case of no polymers for $M = 0.01$ shown in Figure 4 at the same time. However, after breakthrough, a band of high polymer concentration helps increase viscosity ratio and thus saturation relative to the reference case

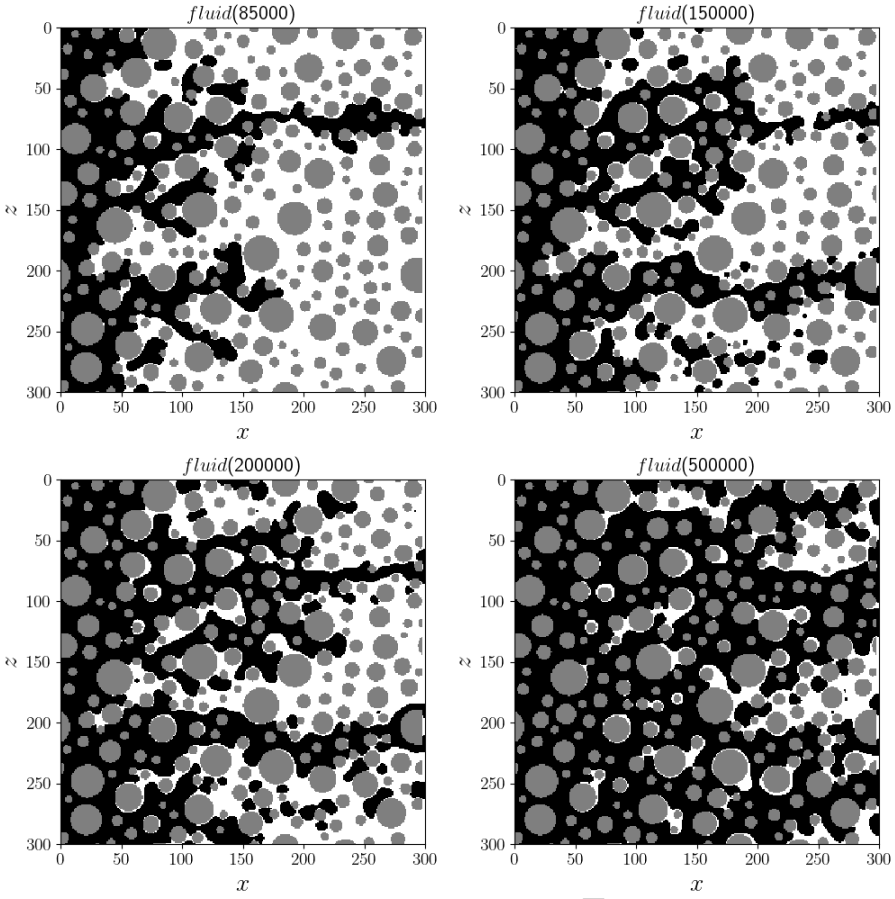

Fig. 4 Snapshots of two phase flow in a porous matrix of a perfectly non-wetting fluid with a viscosity ratio of $M = 0.01$, so in the viscous fingering regime. Black regions depict fluid 1, and white regions depict fluid2.

without use of polymers as seen in snapshots at $t = 200K$ and $t = 500K$. Nonetheless, one observes that at $t = 200K$ time steps, the saturation is far lower than that of the reference casewhen always using polymers (ie. viscosity ratio of $M = 1$) shown in Figure 5.

Figure 7 shows snapshots of the polymer concentration for the case of using polymer additives from the start of the waterflooding simulation for the same duration of $\Delta t_{polymer} = t_{br}$. One observes that the high polymer concentration at the water front has the effect of making the water front's viscosity contrast unity, and hence, making the morphology of the injected water be almost identical to the reference case of stable displacement with $M = 1$ shown in Figure 5. For example, one observes that at $t = 200K$, the

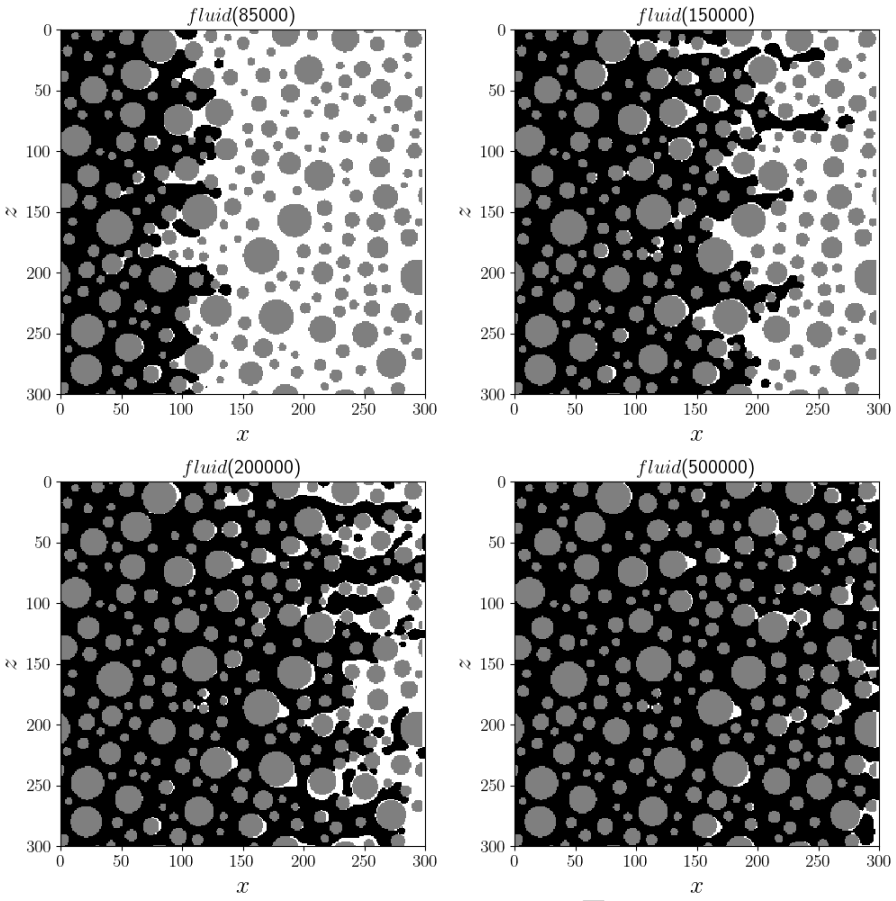

Fig. 5 Snapshots of two phase flow in a porous matrix of a perfectly non-wetting fluid with a viscosity ratio of $M = 1$ (through use of a polymer additive), so in the stable displacement regime. Black regions depict fluid 1, and white regions depict fluid 2.

saturation is very high and certainly much higher than was observed for the case when the polymers were used after breakthrough as shown in Figure 6.

Figure 8 shows the saturation as a function of time for all four cases described above in order to quantify the effect on saturation of using polymers after breakthrough versus from the start, and to compare these cases with the reference cases at a viscosity ratio of $M = 0.01$ and $M = 1$. The plot shows that the saturation versus time for the case for using polymers from the start is almost linear until a high saturation of 90% is reached at 230K time steps, and is almost identical to the case of a viscosity ratio of unity. After this time, the saturation rolls over and only gradually approaches its peak of around 95%. In contrast, the saturation for the case of using polymers after breakthrough slows immediately after breakthrough, as did the reference case of no poly-

mers for $M = 0.01$, but gradually increases above the saturation for the case of no polymers, eventually reaching a 90% saturation after 320K time steps, around 40% longer than it took to reach this saturation when polymers were used from the start. However, although the saturation profile for the case of polymers after breakthrough was far inferior to the case of polymers from the start, it remains much superior to the case of no polymers.

5.4 Comment on addition of polymer adsorbtion

We note that in future research, it should be easy to incorporate adsorption of the polymer onto the rock matrix, provided one knows the isotherm equation for the adsorption process. For example, for linear-reversible adsorption, at each time step for lattice sites adjacent solid sites, one would need to transfer a small amount of the polymer concentration from the fluid solution to the solid surface so that the local isotherm $s = K_d C$ is satisfied, where s is the adsorbed concentration and K_d is the partition coefficient. This process would result in the classic retardation of the fluid concentration front as a result of the additional storativity for the solute in the porous medium. This is not a component of the current paper and is only noted to explain that such extensions to the current work should be relatively straightforward.

5.5 Computational cost

The three-component two-phase RK LBM presented here is around four times more computationally intensive than a single-phase LBM due to the combination of the need to model three components, plus the additional collision term necessary to encourage color separation (ie. cohesive forces) as well as the recoloring step which achieves immiscible flow. Specifically, each of the three componenents requires a streaming and collision step which leads to a factor of three more computationally expensive than single component flow. And the extra collision term for cohesion has a similar cost as the other streaming plus collision steps, so the total computational cost of the two phase three component colour gradient LBM is about a factor of four times more expensive than single component flow. This extra cost combined with the need for large scale 3D simulations to obtain quantitative results for industrial applications, will require large multi-core computational facilities.

We note that fluid-fluid displacement in a patterned micromodel cell is intrinsically 3D, and would benefit from a depth-averaged approach (Hele-Shaw lubrication approximation), as has been done in earlier works for two-phase immiscible flow (Grosfils et al., 2004[9]; Cueto-Felgueroso and Juanes, 2014[5]; Cueto-Felgueroso et al., 2018[6]) or arguably from a fully 3D simulation setup (e.g., Zhao et al., 2019[40]; Zacharoudiou et al., 2020[39]). While 2D and Hele-Shaw simulations can provide quantitative results within the limitations of 2D or Hele-Shaw and insights that may be applicable to real oilfield studies, we

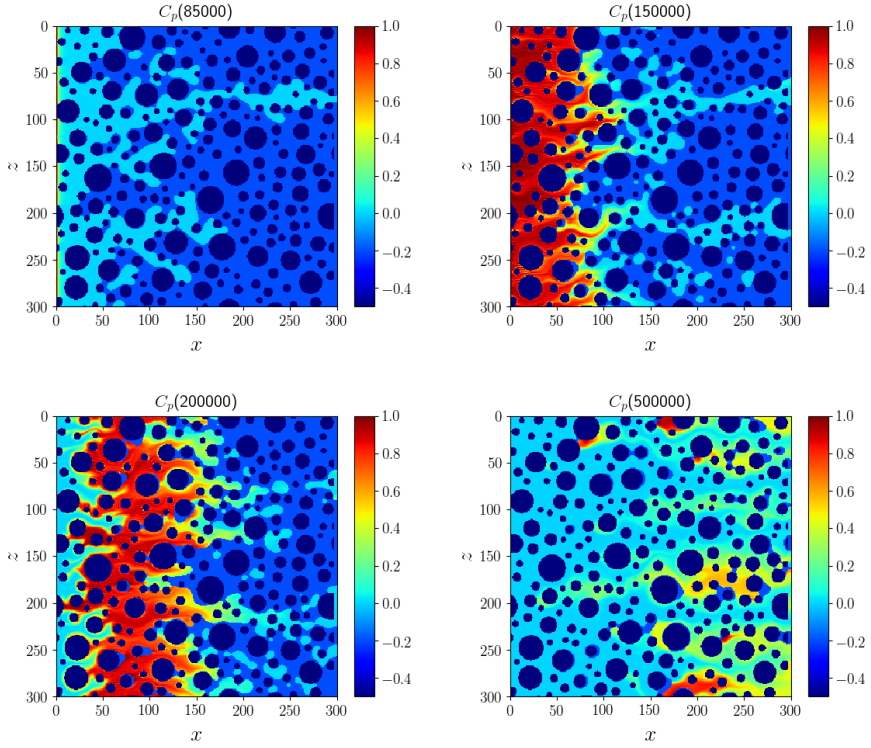

Fig. 6 Snapshots of two phase flow in a porous matrix of a perfectly non-wetting fluid with a viscosity ratio of $M = 0.01$ and polymer injection starting after breakthrough for a duration $\Delta t_{polymer} = t_b$, the breakthrough time for the case with no polymer injection shown in Figure 4. Colours from aqua to red represent polymer concentration, with dark blue representing the grains.

would argue that to obtain quantitative results for practical oilfield studies, it will ultimately necessary to perform large scale fully 3D calculations on powerful parallel computational facilities.

6 Conclusions

We describe a Rothman-Keller two phase LBM that includes modeling of convection-diffusion equation of an additive concentration (eg. polymers) to one of the two fluids, which increases the viscosity of that fluid, and thereby decreases viscous fingering. The method is tested both for merging droplets with different additive concentrations, and for two-phase flow in porous media. We demonstrate the method with 2D simulations of waterflooding experiments at viscosity ratios of $M = 0.01$ and $M = 1$ for reference, and compare these cases to simulations using polymer additives after breakthrough and from the start

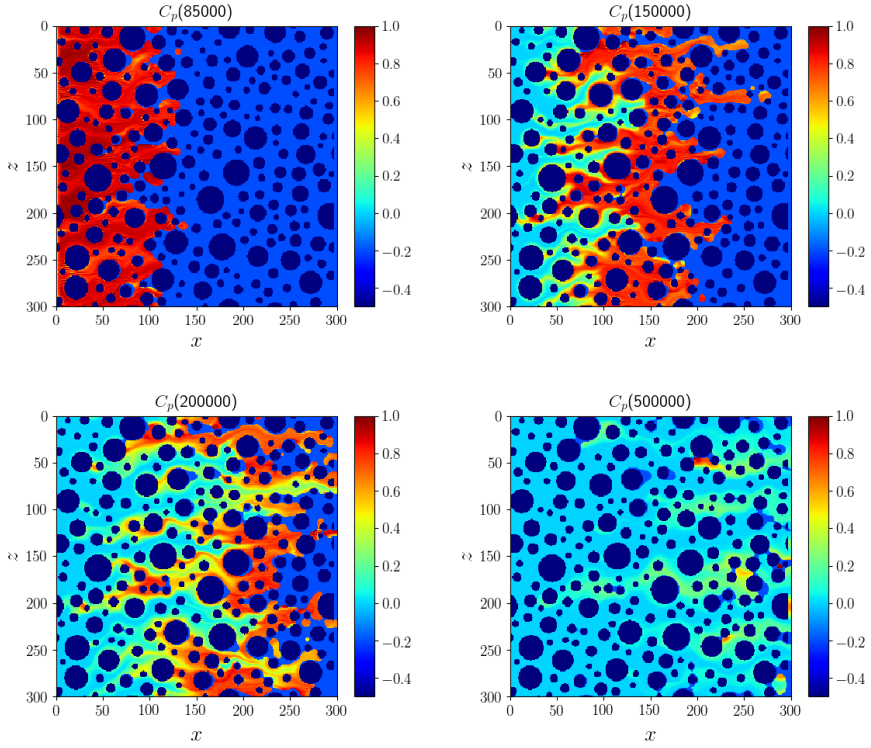

Fig. 7 Snapshots of two phase flow in a porous matrix of a perfectly non-wetting fluid with a viscosity ratio of $M = 0.01$ and polymer injection starting at $t = 0$ for a duration of t_b, the breakthrough time for the case with no polymer injection shown in Figure 4. Colours from aqua to red represent polymer concentration, with dark blue representing the grains.

Fig. 8 Plot of saturation versus time for multi-phase flow in a 2D porous medium with viscosity ratio $M = 0.01$ for the four cases: (1) injection of without any polymer additive (ie. $M = 0.01$), (2) Injection of with 100% concentration with a polymer additive (ie. $M = 1$ always), (3) Injection with a polymer additive after the breakthrough time t_{br} for a duration of $\Delta t_{polymer} = t_{br}$, and (4) Injection of a polymer additive from $t = 0$ for a duration of $\Delta t_{polymer} = t_{br}$.

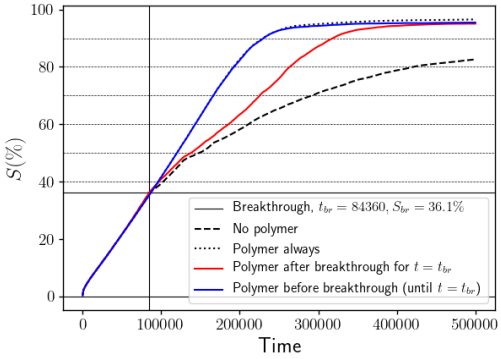

of simulation. The results show that the saturation for the case of using polymer additives from the start largely eliminates the effect of viscous fingering and hence increases saturation greatly relative to the cases of using polymer additives after breakthrough or not at all. Specifically, when polymers are used from the start, the saturation versus time is almost identical to that of using a viscosity ratio of unity (ie. stable displacement). These tests demonstrate that the modified RK color gradient multiphase LBM can be used to study viscous fingering behavior in porous media involving an injected low viscosity fluid which can have its viscosity varied through use of an additive. This is of scientific interest and has economic implications to Enhanced Oil Recovery (EOR) by waterflooding where one aims to maximize oil recovery through optimal use of polymer additives.

7 Acknowledgements

This research was supported by the College of Petroleum Engineering and Geosciences at King Fahd University of Petroleum and Minerals, Saudi Arabia. D.A. Yuen would like to thank National Science Foundations geochemistry and CISE program for support. In addition, this research was in part funded by the US Department of Energy Grant DE-SC0019759 (D.A.Y) by the National Science Foundation (NSF) Grant EAR-1918126 (D.A.Y).

8 Declarations

8.1 Funding

This research was supported by the College of Petroleum Engineering and Geosciences at King Fahd University of Petroleum and Minerals, Saudi Arabia. In addition, this research was funded by the US Department of Energy Grant DE-SC0019759 (D A. Y) by the National Science Foundation (NSF) Grant EAR-1918126 (D.A.Y).

8.2 Conflicts of interest/Competing interests

Not applicable.

8.3 Availability of data and material (data transparency)

Not applicable.

8.4 Code availability (software application or custom code)

Not applicable.

References

1. Abidin, A.Z., Puspasar, T. and Nugroho, W.A. 2012 Polymers for Enhanced Oil Recovery Technology, *Procedia Chemistry*, **4**, pp.11–16, https://doi.org/10.1016/j.proche.2012.06.002
2. Armstrong, R.T., Berg, S., Dinariev, O., Evseev, N., Klemin, D., Koroteev, D. and Safonov, S. 2016 Modeling of Pore-Scale Two-Phase Phenomena Using Density Functional Hydrodynamics, *Transport in Porous Media*, **112**, 577—607.
3. Blunt, M.J., Bijeljic B., Dong H., Gharbi O., Iglauer S., Mostaghimi P, Paluszny A. and Pentland, C. 2013 Pore-scale imaging and modelling, *Advances in Water Resources*, **51**, 197–216.
4. Chen, J.D. and Wilkinson, D. 1985 Pore–scale viscous fingering in porous media, *Phys. Rev. Lett.*, **55**(18), pp.1892–1896.
5. Cueto-Felgueroso, L. and Juanes, R. 2014 A phase-field model of two-phase Hele-Shaw flow, *Journal of fluid mechanics*, **758**, 522–552.
6. Cueto-Felgueroso, L., Fu, X. and Juanes, R. 2018 Pore-scale modeling of phase change in porous media, *Physical Review Fluids*, **3**(8), 084302.
7. Deng, X., Kamal, M.S., Patil, S., Hussain, S.M.S., and Zhou, X. 2020 A review on wettability alteration in catbonate rocks: wettability modifiers, *Energy and Fuels*, **34**, pp.31–54.
8. Demianov A, Dinariev O. and Evseev N. 2011 Density functional modelling in multiphase compositional hydrodynamics, *Can. J. Chem. Eng.*, **89**, 207—226.
9. Grosfils, P., Boon, J. P., Chin, J. and Boek, E. S. 2004 Structural and dynamical characterization of Hele–Shaw viscous fingering, *Philosophical Transactions of the Royal Society of London. Series A: Mathematical, Physical and Engineering Sciences*, **362**(1821), 1723–1734.
10. Grunau, D., Chen, S, and Eggert, K. 1993 A lattice Boltzmann model for multiphase fluid flows, *Physics of Fluids A: Fluid Dyanmics*, **5**(10), pp.2557–2562.
11. Gunstensen, A.K., Rothman, D.H., Zeleski, S. and Zanetti, G. 1991 Lattice Boltzmann model of immiscible fluids, *Physical Review A*, **43**(8), pp.4320–4327.
12. He, X., Chen, S. and Zhang, R. 1999 A lattice Boltzmann scheme for incompressible multiphase flow and its application in simulation of Rayleigh–Taylor instability, *Journal of computational physics*, **152** (2), 642–663.
13. Homsy, G.M. 1997 Viscous fingering in porous media, *Ann. Rev. Fluid Mech.*, **19**, pp.271–311.
14. Huang, H., Sukop, M. and Lu, X. 2015 Multiphase lattice Boltzmann methods: Theory and application, John Wiley & Sons, 371pp.
15. Inamuro, T., Ogata, T., Tajima, S. and Konishi, N. 2004 A lattice Boltzmann method for incompressible two-phase flows with large density differences, *Journal of Computational physics*, **198** (2), 628–644.
16. Jadhunandan, P.P. and Morrow, N.R. 1995 Effect of wettability on waterflood recovery for crude-oil/brine/rock systems, *SPE Reserv. Eng.*, **10**, pp.40–46.
17. Kennedy, H.T., Burja, E.O. and Boykin, R.S. 1955 An investigation of the effects of wettability on the recovery of oil by water flooding, *J. Phys. Chem.*, **59**, pp.867–879.
18. Krüger, T., , Kusumaatmaja, H., Kuzmin, O., The Lattice Boltzmann Method: Principles and Practice (Chapter 8), Springer, 10.1007/978-3-319-44649-3_8
19. Latva-Kokko, M. and Rothman, D. 2005 Static contact angle in lattice Boltzmann models of immiscible fluids, *Phys. Rev. E*, **74**(4), 046701.
20. Leclaire, S., Reggio, M. and Trépanier, J-Y. 2011 Isotropic color gradient for simulating very high-density ratios with a two-phase flow lattice Boltzmann model, *Computers and Fluids*, **48**(1), pp.98–112.
21. Lenormand, R., Touboul, E. and Zarcone, C. 1988 Numerical models and experiments on immiscible displacements in porous media, *J. Fluid Mech.*, **1989**, pp.165–187.
22. Måløy, K.J., Feder, J. and Jøssang 1985 Viscous fingering fractals in porous media, *Phys. Rev. Lett.*, **55**(24), pp.2688–2691.
23. Mora, P., Morra, G. and Yuen, D. 2021a Optimal surface tension isotropy in the Rothman-Keller colour gradient Lattice Boltzmann Method for multi-phase flow, *Phys. Rev. E*, **103**(3), 033302, https://doi.org/10.1103/PhysRevE.103.033302.

24. Mora, P., Morra, G., Yuen, D. and Juanes, R. 2021b Optimal wetting angles in Lattice Boltzmann simulations of viscous fingering, *Transport in Porous Media*, **136**, 831-–842, https://doi.org/10.1007/s11242-020-01541-7.
25. Mora, P., Morra, G.,Yuen, D. and Juanes, R. 2021c Influence of wetting on viscous fingering via 2D Lattice Boltzmann simulations, Transport in Porous Media, **138**, 511–538, doi=https://doi.org/10.1007/s11242-021-01629-8.
26. Morrow, N. and Buckley, J. 2011 Improved oil recovery by low salinity waterflooding, *J. Pet. Technol.*, **63**, pp.106-112.
27. Reis, T. and Phillips, T.N. 2007 Lattice Boltzmann model for simulating immiscible two-phase flows, *J. of Physics A: Mathematical and Theoretical*, **40**(14), pp.4033–4053.
28. Rothman, D. and Keller, J. 1988 Immiscible cellular automaton fluids, *J. Stat. Phys.*, **52**(3/4), pp.1119–1127.
29. Seethepalli, A., Adibhatla, B. and Mohanty, K.K. 2004 Physicochemical interactions during surfactant flooding of fractured carbonate reservoirs, *SPE J.*, **9**(4), pp.411–418, doi=10.2118/89423-PA.
30. Shan, X. and Chen, H. 1993 Lattice Boltzmann model for simulating flows with multiple phases and components, *Physical review E*, **47** (3), 1815.
31. Swift, M.R., Orlandini, E., Osborn, W.R. and Yeomans, J.M. 1996 Lattice Boltzmann simulations of liquid-gas and binary fluid systems, *Physical Review E*, **54** (5), 5041.
32. Trojer, M., Szulczewski, M.L. and Juanes, R. 2015 Stabilizing fluid–fluid displacements in porous media through wettability alteration, *Phys. Rev. Appl.*, **3**(5), 054008.
33. Wang, H., Yuan, X., Liang, H., Chai, Z. and Shi, B. (2019) A brief review of the phase-field-based lattice Boltzmann method for multiphase flows, *Capillarity*, **2** (3), 33 – 52.
34. Yakimchuk, I., Evseev, N., Korobkov, D., Ridzel, O. and Pletneva V. (2020), Study of Polymer Flooding at Pore Scale by Digital Core Analysis for East-Messoyakhskoe Oil Field, SPE Russian Petroleum Technology Conference, Virtual, October 2020, Paper Number: SPE-202013-MS, https://doi.org/10.2118/202013-MS
35. Yang, J. and Boek, E.S. 2013 A comparison study of multi-component Lattice Boltzmann models for flow in porous media applications, *Computers Mathematics with Applications*, **65** (6), 882–890.
36. Zhang, Z., Li, Z. and Wu, W. 2022 Advection-diffusion Lattice Boltzmann Method with and without dynamical filter, *Frontiers in physics*, **10**, 875628.
37. Zhao, B., MacMinn, C.W. and Juanes, R. 2016 Wettability control on multiphase flow in patterned microfluidics, *Proc. Natl Acad. Sci. USA*, **113**(37), pp.10251–10256.
38. Zou, Q. and He, X. 1997 On pressure and velocity flow boundary conditions and bounce back for the lattice Boltzmann BGK model, *Physics of Fluids*, **9**, pp.1591–1598.
39. Zacharoudiou, I., Boek, E.S. and Crawshaw, J. 2020 Pore-scale modeling of drainage displacement patterns in association with geological sequestration of CO2, *Water resources research*, **56** (11), doi.org/10.1029/2019WR026332.
40. Zhao, B., MacMinn, C. W., Primkulov, B. K., Chen, Y., Valocchi, A. J., Zhao, J., . . . and Juanes, R. 2019 Comprehensive comparison of pore-scale models for multiphase flow in porous media, *Proceedings of the National Academy of Sciences*, **116**(28), 13799–13806.